Supporting information

Hollow Au Nanorattles for Boosting the Performance of Organic Photovoltaics

Zhi Yong Bao,[ab,#] Shenghua Liu,[b,#] Yidong Hou,[d,#] Aixue Shang,[b] Feng Yan,[b,*] Yucheng Wu,[a] Dangyuan Lei,[c,*] Jiyan Dai[b,*]

[a] *School of Materials Science and Engineering, Hefei University of Technology, Hefei, China*
[b] *Department of Applied Physics, The Hong Kong Polytechnic University, Hong Kong, China*
[c] *Department of Materials Science and Engineering, City University of Hong Kong, Hong Kong*
[d] *School of Physical Science and Technology, Sichuan University, Chengdu, Sichuan, China*

E-mail: *feng.yan@polyu.edu.hk
*dangylei@cityu.edu.hk
* jiyan.dai@polyu.edu.hk

Table of contents

Fig. S1 The schematic diagram to illustrate the structures of hollow Au nanorattles.

Fig. S2 The simulated charge distribution of longitudinal LSPR modes for the S, M and L-nanorattles.

Fig. S3 The simulated longitudinal extinction spectra of S, M and L-nanorattles.

Fig. S4 SEM images of Au nanorattles spin-coated onto the pre-cleaned ITO/glass substrates.

Fig. S5 SEM images of Au nanorattles (1, 3, 6 and 10 vol. %) on ITO/glass substrates.

Fig. S6 The spectral matching between PTB7 and L-NRs (a); PBDTTT and S-NRs (b).

Fig. S7 The near-field intensity and the field distribution of discrete S-NR (a and c) and L-NR (b and d) in PTB7. (a), (b) for the longitudinal and (c), (d) for the transverse resonant wavelengths.

Fig. S8 The near-field intensity and the field distribution of discrete S-NR (a and c) and L-NR (b and d) in PBDTTT. (a), (b) for the longitudinal and (c), (d) for the transverse resonant wavelengths.

Fig. S9 TEM images of Au@SiO_2 nanorattle samples (S-NRs). The red marks show the thin SiO_2 shell a little defective.

Fig. S10 J-V curves of the best and control OPVs device based on PBDTTT-EFT:PC71BM with incorporation of Au@SiO_2 nanorattles (S-NRs) in active layer (6.0 vol.% solution volume percentage).

Materials and Experiment Characterization

Materials

Chemicals: cetyltrimethylammonium bromide (CTAB), tetrachloroauric (III) acid ($HAuCl_4$), cetyltrimethylammonium chloride (CTAC), silver nitrate ($AgNO_3$), ascorbic acid (AA), trisodium citrate, sodium borohydride, L-cysteine, D-cysteine, and DL-cysteine were purchased from Sigma. All chemicals were used without further purification. Ultrapure water was used for all experiments. Polythieno[3,4-b]-thiophene-benzodithiophene(PTB7), [6,6]-phenyl C71-butyric acid methylester(PC71BM) and poly[4,8-bis(5-(2-ethylhexyl)thiophen-2-yl)-benzo[1,2-b;4,5-b'] dithiophene-2,6-diyl-alt-(4-(2-ethylhexyl)-3-fluorothieno[3,4-b]thiophene-)-2-carboxylate-2- 6-diyl)] (PBDTTT-EFT) were purchased from 1-Materials Inc. The poly(3,4- ethylenedioxythiophene):polystyrene sulphonic acid (PEDOT:PSS) (Clevios™ P VP AI 4083) was purchased from Heraeus, Germany.

Instrument and characterization

The extinction spectra of the aqueous solution containing Au nanorattles with different gap thicknesses were characterized by using a UV-VIS spectrophotometer (UV-2550, Shimadzu, Japan). The prepared nanostructures were drop-casted on a TEM

grid to perform high-resolution morphology characterization and EDX element mapping using a JEM2100F TEM system operating at 300 kV.

Syntheses of Au nanorods, Ag@Ag nanocuboids and hollow Au nanorattles

Firstly, Au nanorods were synthesized by using a seed-mediated method.[1] Seed solution was synthesized by adding 0.6 mL of an ice-cold $NaBH_4$ (10 mM) solution into 10 mL of $HAuCl_4$ (0.25 mM) and CTAB (0.1 M) solution under vigorous stirring at room temperature. The color of the seed solution changed from yellow to brown. Growth solution was prepared by mixing 5 mL of $HAuCl_4$ (10 mM), 95 mL of CTAB (0.1 M), 1 mL of $AgNO_3$ (10 mM) and 0.55 mL of AA (0.1 M), consecutively. The solution was homogenized by gentle stirring. Then 0.10 mL of freshly prepared seed solution was added to the colorless solution and kept undisturbed in dark at least 12 h. Before use, the Au nanorods solution was centrifuged twice at 7000 rpm for 15 min to remove excess CTAB and finally re-dispersed in DI water.

The Au@Ag core-shell nanocuboids were prepared according to a reported procedure with appropriate modifications.[2] Specifically, 5 mL of the Au NRs solution were centrifuged and re-dispersed into an aqueous CTAC solution (0.08 M) at the same volume. Then, 0.6, 1.2 and 2.0 mL of $AgNO_3$ (0.01 M) were subsequently added into four Au nanorods solutions of 6 mL, followed by respective addition of 0.3, 0.6 and 1.0 mL ascorbic acid solutions (0.1 M). The resultant solutions were kept in an isothermal oven at 65 °C for 4.5 h.

Au nanorattles were synthesized by transforming Ag shell of Au@Ag nanocuboids into Au shell via galvanic replacement reaction.[3] The as synthesized Au@Ag nanocuboids were centrifuged and redispersed in CTAC solution (40 mM), followed by heating at 80 °C for 3 min under magnetic stirring. $HAuCl_4$ aqueous solution (0.2 mM) was injected into the Au@Ag solution at a rate of 0.6 mL/min under magnetic stirring. Then Au nanorattle aqueous solutions (~2×10^{-10} M) with three different gap thicknesses (2.1, 6.6 and 12.4 nm) were prepared. The sizes of the Au cores in the experiment were kept identical.

Device fabrication

Three types of newly synthesized Au nanorattle solutions were introduced into PEDOT:PSS aqueous solution with various volume ratios(1, 3, 6 and 10 vol. %). Then PEDOT:PSS hole transport layers of OPVs were prepared by coating the solutions on substrates. For conventional bulk heterojunction (BHJ) structure shown in Figure 2a, the pristine and Au nanorattles introduced PEDOT:PSS were spincoated onto the pre-cleaned ITO/glass substrates at 4000 rpm for 40 seconds (after O_2 plasma treatment for 6 min) and heated at 150 ^oC for 1 h. While for the device structure of ITO/PEDOT:PSS/Au@SiO_2 nanorattles+active layer, Au nanorattle ethanol solutions with the same concentration (~2×10^{-10} M) were spin-coated on the pristine PEDOT:PSS layer at the spin coating speed of 4000 rpm for 40 seconds, followed by 70℃ annealing for 5 mins. After that, the blend precursor of PTB7 and $PC_{71}BM$ (1:1.5 wt-ratio for 25 mg/ml) in the mixed solvents of chlorobenzene (CB) and 1,8-diiodoctane (DIO)

(97%:3% in volume) was spin-cast on top of the PEDOT:PSS film at 1500 rpm for 1 min, followed by slow drying. Then, methanol was spin-coated onto the active layer at 2500 rpm for 60 seconds. Finally, a 20 nm-thick Ca layer and a 100 nm Al electrode were successively deposited on the active layer by thermal evaporation. The area of the active layer defined by the Al and ITO electrodes of the device was 8.0 mm^2. All of the OPVs were then encapsulated in the glove box and tested in air. All the preparation conditions of the OPVs based on PBDTTT-EFT:$PC_{71}BM$ were exactly the same as PTB7:$PC_{71}BM$ -based devices as described above.

Electromagnetic simulations

The full-wave simulations were conducted with a commercial finite-element solver (Comsol Multiphysics 4.3a with RF module), which is commonly used to simulate the LSPR of plasmonic nanoparticles. When performing the numerical simulations, the total-field scattering-field source was used to get the extinction cross sections as well as the electric field distributions at the longitudinal and transverse resonant wavelengths. In all calculations, the frequency dependent permittivity of Au and Ag were modeled using the experimental data of Johnson and Christy with linear interpolation. The simulation domain was finely meshed with the smallest size of 1.5 nm in the metal region to ensure the accuracy of the calculated results.

Conditions	V_{oc} (V)	J_{sc} (mA/cm^2)	FF (%)	PCE (%)	PCE enhancement
	0.726	16.15	67.5	7.91	Control
1.0 vol.%	0.732	16.87	67.5	8.33	5.31% Best
	0.731	16.72	65.9	8.06	1.90% Average
3.0 vol.%	0.735	17.13	65.7	8.27	4.55% Best
	0.730	17.22	65.2	8.19	3.54% Average
6.0 vol.%	0.735	16.92	67.2	8.36	5.69% Best
	0.732	16.99	66.6	8.28	4.68% Average
10.0 vol.%	0.725	16.89	67.4	8.25	4.30% Best
	0.726	16.81	65.7	8.02	1.4% Average

Table S1 Summary of photovoltaic performance of OPVs based on PTB7:$PC_{71}BM$ with different addition levels (solution volume percentage) of Au nanorattless in PEDOT:PSS. (*gap thickness is 2.1 nm*)

Conditions	V_{oc} (V)	J_{sc} (mA/cm^2)	FF (%)	PCE (%)	PCE enhancement
	0.779	17.72	65.7	9.07	Control
1.0 vol.%	0.796	18.01	67.4	9.66	6.50% Best
	0.788	18.05	67.3	9.57	5.51% Average
3.0 vol.%	0.792	18.35	67.5	9.81	8.16% Best
	0.787	18.24	67.7	9.72	7.17% Average
6.0 vol.%	0.789	19.25	69.5	10.55	16.3% Best
	0.786	19.27	68.9	10.43	14.99% Average
10.0 vol.%	0.781	18.19	69.0	9.80	8.05% Best
	0.777	18.10	68.6	9.65	6.40% Average

Table S2 Summary of photovoltaic performance of OPVs based on PBDTTT-EFT:$PC_{71}BM$ with different addition levels (solution volume percentage) of Au nanorattles in PEDOT:PSS. (*gap thickness is 2.1 nm*)

Conditions	V_{oc} (V)	J_{sc} (mA/cm^2)	FF (%)	PCE (%)	PCE enhancemenet
	0.726	16.15	67.5	7.91	Control
Gap 2.1 nm	0.735	16.92	67.2	8.36	5.69% Best
	0.732	16.99	66.6	8.28	4.68% Average
Gap 6.6 nm	0.731	17.81	66.7	8.68	9.73% Best
	0.729	17.60	67.0	8.60	8.72% Average
Gap 12.4 nm	0.728	17.80	67.9	8.80	11.25% Best
	0.729	17.75	67.5	8.73	10.37% Average

Table S3 Summary of photovoltaic performance of OPVs based on PTB7:$PC_{71}BM$ with different gap thickness (2.1, 6.6 and 12.4 nm) of Au nanorattles in PEDOT:PSS. (6.0 vol.% solution volume percentage)

Conditions	V_{oc} (V)	J_{sc} (mA/cm^2)	FF (%)	PCE (%)	PCE enhancement
	0.779	17.72	65.7	9.07	Control
Gap 2.1 nm	0.789	19.25	69.5	10.55	16.31% Best
	0.786	19.27	68.9	10.43	14.99% Average
Gap 6.6 nm	0.795	18.74	65.7	9.79	7.94% Best
	0.790	19.00	64.8	9.72	7.17% Average
Gap 12.4 nm	0.778	18.09	68.7	9.67	6.62% Best
	0.783	18.02	67.2	9.48	4.52% Average

Table S4 Summary of photovoltaic performance of OPVs based on PBDTTT-EFT:$PC_{71}BM$ with different gap thickness (2.1, 6.6 and 12.4 nm) of Au nanorattles in PEDOT:PSS. (6.0 vol.% solution volume percentage)

Conditions	V_{oc} (V)	J_{sc} (mA/cm^2)	FF (%)	PCE (%)	PCE Enhancement
Control	0.80	16.74	69.9	9.36	Control
Au@SiO_2 Gap:2.1 nm nanorattles	0.80	18.32	73.3	10.74	14.74% Average
	0.80	18.56	72.9	10.82	15.60% Best

Table S5 Summary of photovoltaic performance of OPVs based on PBDTTT-EFT:PC71BM with incorporation of Au@SiO_2 nanorattles (S-NRs) in active layer (6.0 vol.% solution volume percentage).

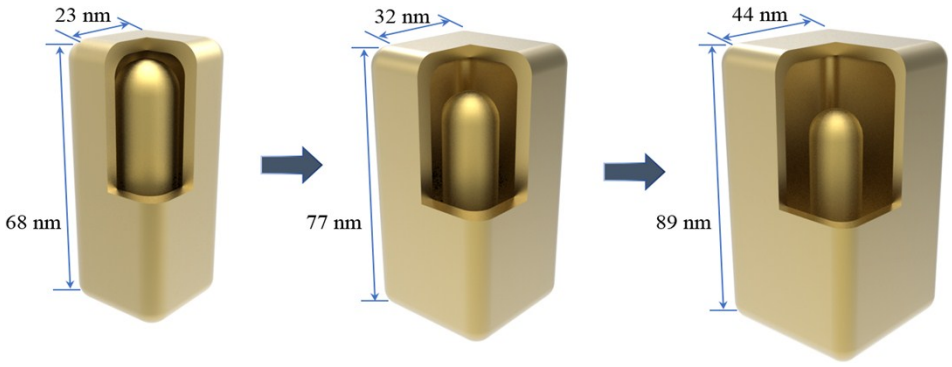

Fig. S1 The schematic diagram to illustrate the structures of hollow Au nanorattles.

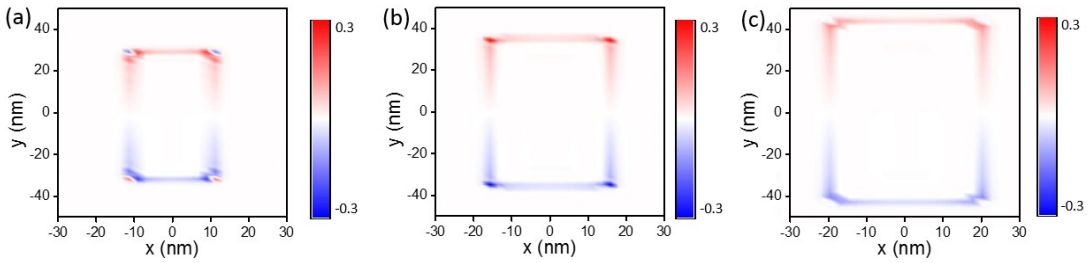

Fig. S2 The simulated charge distribution of longitudinal LSPR modes for the S, M and L-nanorattles.

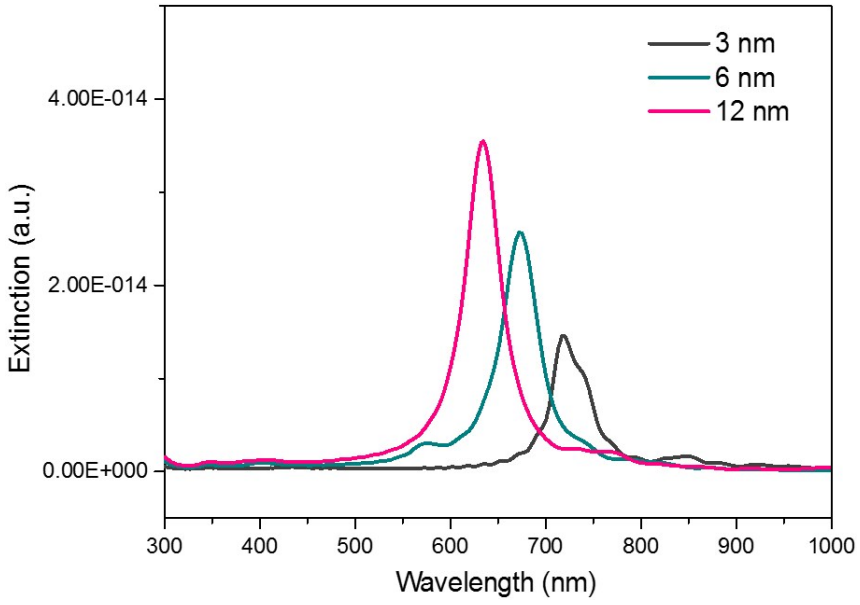

Fig. S3 The simulated longitudinal extinction spectra of S, M and L-nanorattles.

In Fig. 1g, the absorption peak at ~700 nm for Au nanorattles is attributed to the longitudinal localized surface plasmon resonances (LSPRs) dipole mode (which is similar to the Au nanorods). The is verified by our additional simulations as shown in

Fig. S2. In fact, the length and width of the nanorattles are at the same nanoscale, therefore, the charge distribution in the long axis and the short axis is not completely independent. The presented longitudinal LSPR peak is not only dependent on the sizes of the Au nanorattles, but also associated with the aspect ratio of the nanorattles. As the Au+ precursor is provided, both the diameters and lengths of Au nanorattles increase. When the gap sizes refer to 2.1, 6.6 and 12.4 nm, the aspect ratio of nanorattles can be calculated as ~2.96, 2.41 and 2.02, respectively. Besides, the coupling effect between the Au core and Au shell may be negligible since there is a thin Au sheet linker (shown in Figs. 1d, 1e and 1f). As a result, the measured longitudinal LSPR blue-shifts with the increase of interior gap size. To further elaborate this point, we calculate their longitudinal LSPR peaks with the corresponding nanoparticle sizes. As can be seen in Fig. S3, the simulated results of blue-shift trend are consistent with the experimental cases.

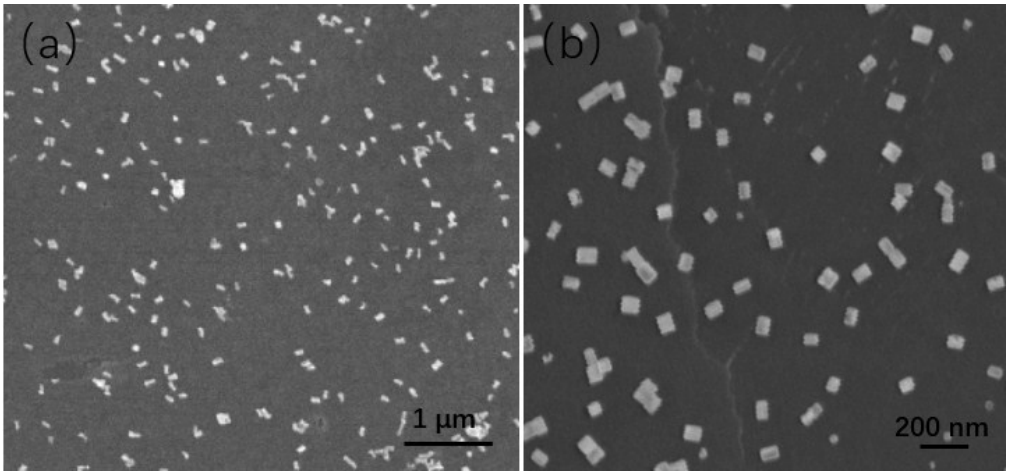

Fig. S4 SEM images of Au nanorattles spin-coated onto the pre-cleaned ITO/glass substrates.

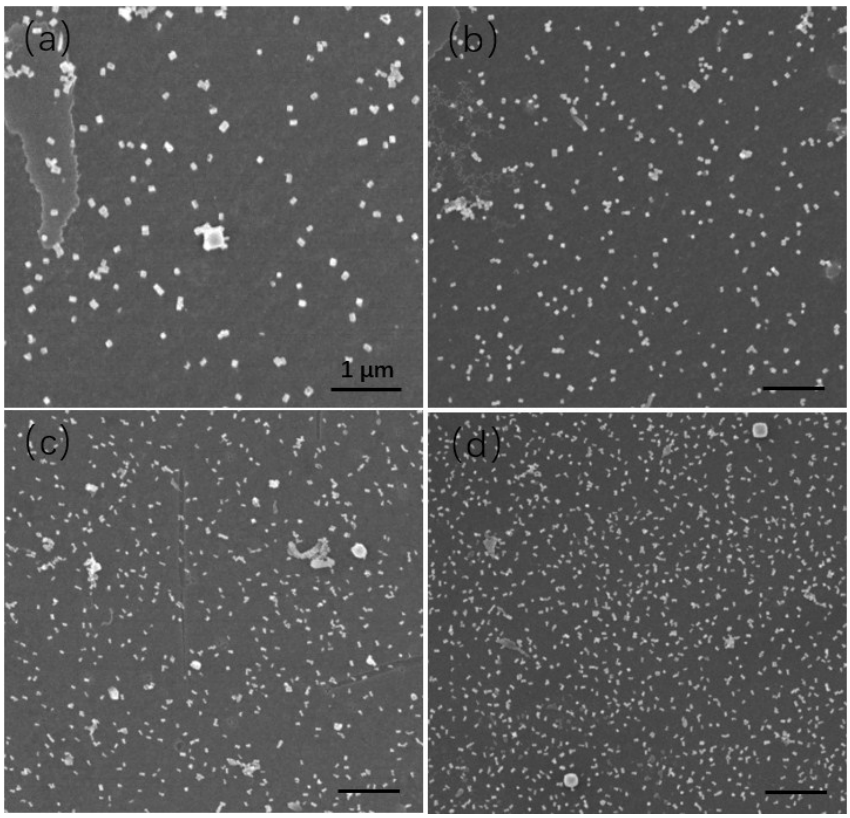

Fig. S5 SEM images of Au nanorattles (1, 3, 6 and 10 vol. %) on ITO/glass substrates.

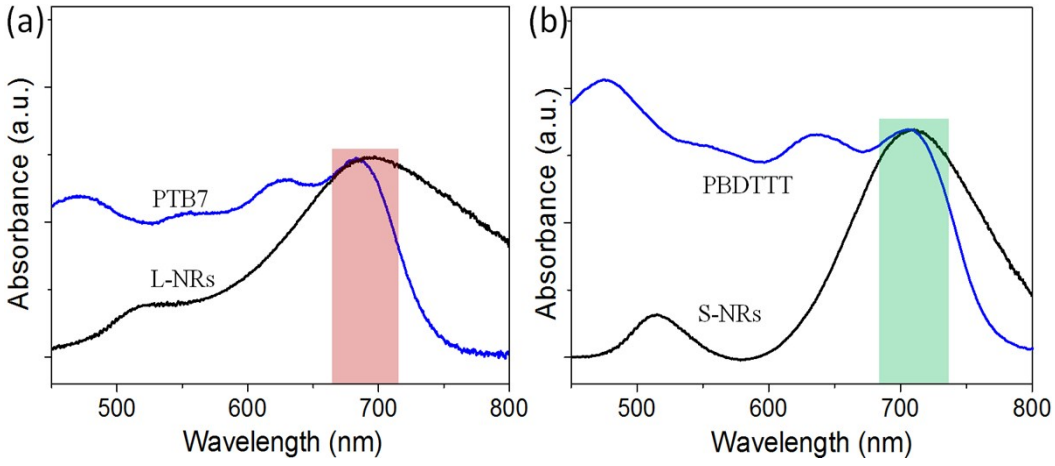

Fig. S6 The spectral matching between PTB7 and L-NRs (a); PBDTTT and S-NRs (b).

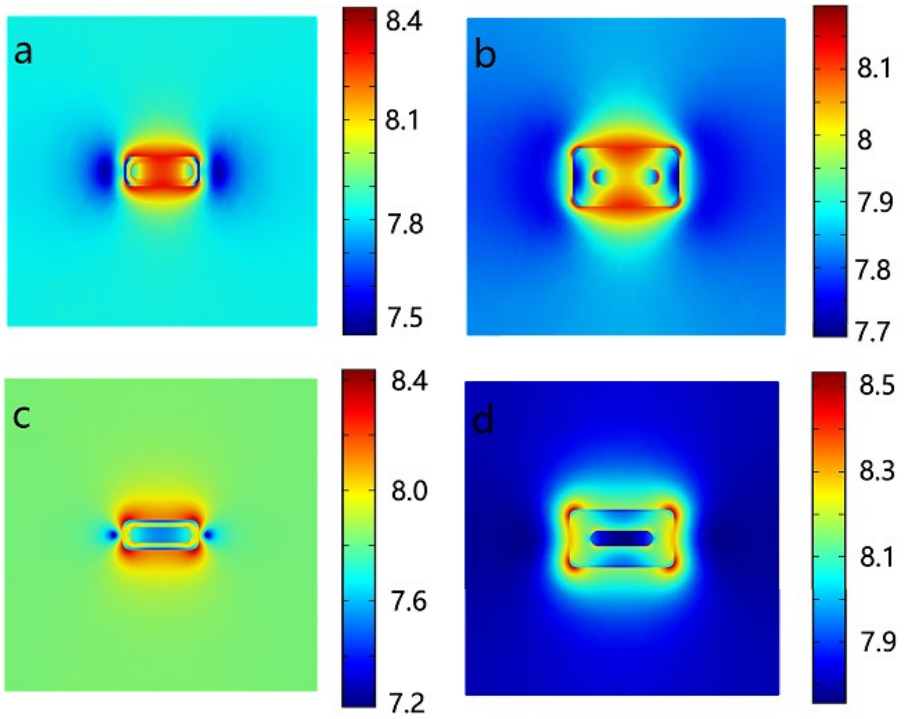

Fig. S7 The near-field intensity and the field distribution of discrete S-NR (a and c) and L-NR (b and d) in PTB7. (a), (b) for the longitudinal and (c), (d) for the transverse resonant wavelengths.

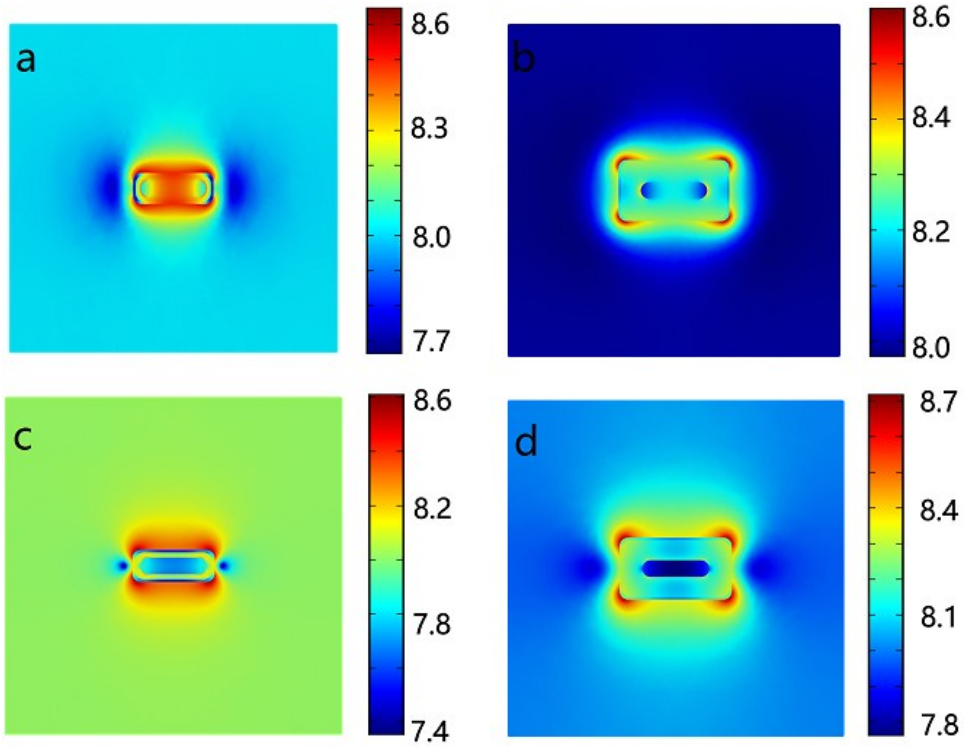

Fig. S8 The near-field intensity and the field distribution of discrete S-NR (a and c) and L-NR (b and d) in PBDTTT. (a), (b) for the longitudinal and (c), (d) for the transverse resonant wavelengths.

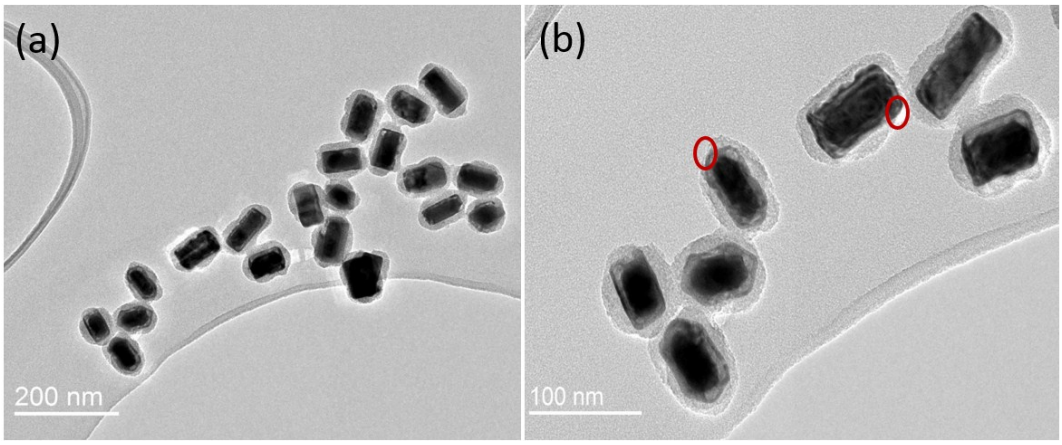

Fig. S9 TEM images of $Au@SiO_2$ nanorattle samples (S-NRs). The red marks show the thin SiO_2 shell a little defective.

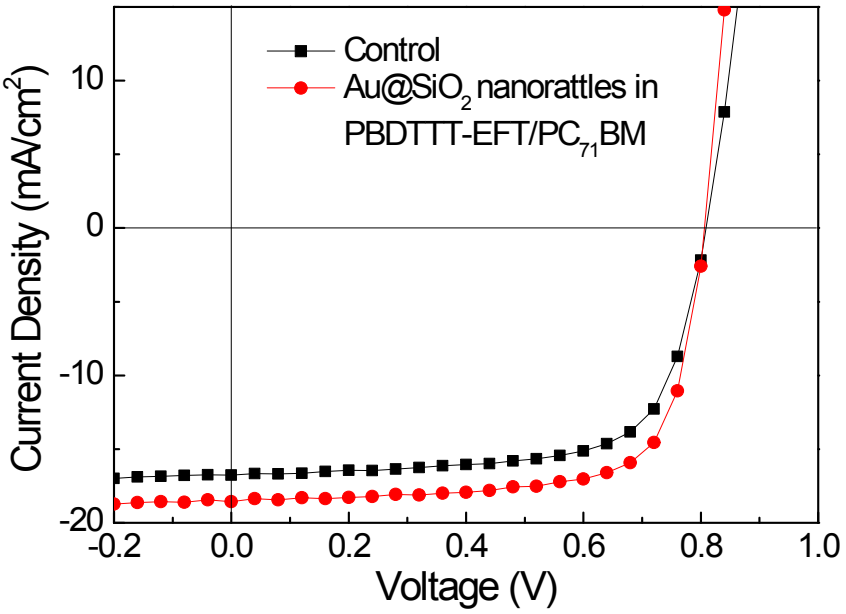

Fig. S10 J-V curves of the best and control OPVs device based on PBDTTT-EFT:PC71BM with incorporation of $Au@SiO_2$ nanorattles (S-NRs) in active layer (6.0 vol.% solution volume percentage).

To further elaborate the plasmonic near-field effect, we coated a ~5-nm SiO_2 shell outside the Au nanorattles through the Stöber method (*J. Colloid Interface Sci.,* 1968, **26,** 62) and investigated the OPV efficiencies by incorporating these $Au@SiO_2$ nanorattles in the active layer. The average enhancement factor of the $Au@SiO_2$ nanorattle-incorporated OPVs (14.74%) is comparable to that of devices with incorporation of bare Au nanorattles in PEDOT:PSS layer (14.99%), as shown in Fig. S10. The reasons why we have not seen a larger enhancement factor in the $Au@SiO_2$ nanorattle-incorporated OPVs may be ascribed as following: 1) the thickness of SiO_2 is

important since the plasmonic near-field is dependent on distance between the Au nanorattle and the polymer. Therefore, it is necessary to optimize the coated thickness of SiO_2; 2) The prepared thin SiO_2 shell may be a little defective (the red marks shown in Fig. S9), which could increase the contact chance between the organic active layer and nanorattles. Therefore, the recombination of photo-generated charges increases and the enhancement factor decreases.

References:

1 Z. Y. Bao, D. Y. Lei, R. Jiang, X. Liu, J. Dai, J. Wang, L. W. C. Helen and Y. H. Tsang, *Nanoscale,* 2014, **6**, 9063.

2 Z. Y. Bao, W. Zhang, Y.-L. Zhang, J. He, J. Dai, C.-T. Yeung, G.-L. Law, and D. Y. Lei, *Angew. Chem. Int. Ed*., 2017, **56**, 1283.

3 K.-K. Liu, S. Tadepalli, L. Tian, S. Singamaneni, *Chem. Mater*., 2015, **27**, 5261.